


Modelling three-dimensional cancer-associated cachexia and therapy: The molecular basis and therapeutic potential of interleukin-6 transsignalling blockade

Marianna Cosentino¹, Laura Forcina¹, Mariam Zouhair¹, Ludovica Apa², Desirée Genovese¹, Caterina Boccia¹, Emanuele Rizzuto² & Antonio Musarò^{1,3*} 

¹DAHFMO-Unit of Histology and Medical Embryology, Sapienza University of Rome, Laboratory affiliated to Istituto Pasteur Italia – Fondazione Cenci Bolognetti, Rome, Italy;

²Department of Mechanical and Aerospace Engineering, Sapienza University of Rome, Rome, Italy; ³Scuola Superiore di Studi Avanzati Sapienza (SSAS), Sapienza University of Rome, Rome, Italy

Abstract

Background Causes and mechanisms underlying cancer cachexia are not fully understood, and currently, no therapeutic approaches are available to completely reverse the cachectic phenotype. Interleukin-6 (IL-6) has been extensively described as a key factor in skeletal muscle physiopathology, exerting opposite roles through different signalling pathways.

Methods We employed a three-dimensional ex vivo muscle engineered tissue (X-MET) to model cancer-associated cachexia and to study the effectiveness of selective inhibition of IL-6 transsignalling in counteracting the cachectic phenotype. Conditioned medium (CM) derived from C26 adenocarcinoma cells was used as a source of soluble factors contributing to the establishment of cancer cachexia in the X-MET model. A dose of 1.2 ng/mL of glycoprotein-130 fused chimaera (gp130Fc) was added to cachectic culture medium to neutralize IL-6 transsignalling.

Results C26-conditioned medium induced a cachectic-like phenotype in the X-MET, leading to a decline of muscle mass (−60%; $P < 0.001$), a reduction in myosin expression (−92.4%; $P < 0.005$) and a reduction of the contraction frequency spectrum (−94%). C26-conditioned medium contains elevated amounts of IL-6 (8.61 ± 4.09 pg/mL) and IL6R (56.85 ± 10.96 pg/mL). These released factors activated the signal transducer and activator of transcription 3 (STAT3) signalling in the C26_CM X-MET system (phosphorylated STAT3/TOTAL +54.6%; $P < 0.005$), which in turn promote an enhancement of IL-6 (+69.2%; $P < 0.05$) and Il6r (+43%; $P < 0.05$) gene expression, suggesting the induction of a feed-forward loop. The selective neutralization of IL-6 transsignalling, by gp130Fc, in C26_CM X-MET prevented the hyperactivation of STAT3 (−55.8%; $P < 0.005$), countered the reduction of cross-sectional area (+28.2%; $P < 0.05$) and reduced the expression of proteolytic factors including muscle ring finger-1 (−88%; $P < 0.005$) and ATROGIN1 (−92%; $P < 0.05$), thus preserving the robustness and increasing the contractile force (+20%) of the three-dimensional muscle system. Interestingly, the selective inhibition of IL-6 transsignalling modulated gene regulatory networks involved in myogenesis and apoptosis, normalizing the expression of pro-apoptotic miRNAs, including miR-31 (−53.2%; $P < 0.05$) and miR-34c (−65%; $P < 0.005$), and resulting in the reduction of apoptotic pathways highlighted by the sensible reduction of cleaved caspase 3 (−92.5%; $P < 0.005$) in gp130Fc-treated C26_CM X-MET.

Conclusions IL-6 transsignalling appeared as a promising target to counter cancer cachexia-related alterations. The X-MET model has proven to be a reliable drug-screening tool to identify novel therapeutic approaches and to test them in preclinical studies, significantly reducing the use of animal models.

Keywords cancer cachexia; drug screening; IL-6 transsignalling blockade; muscle wasting; three-dimensional skeletal muscle model

Received: 1 December 2022; Revised: 19 July 2023; Accepted: 21 August 2023

*Correspondence to: Antonio Musarò, Unit of Histology and Medical Embryology, Sapienza University of Rome, Via A. Scarpa, 14, Rome 00161, Italy.
Email: antonio.musaro@uniroma1.it

Marianna Cosentino and Laura Forcina contributed equally to this work.

Funding information This research was funded by Fondazione Roma, Agenzia Spaziale Italiana (ASI) (MARS-PRE-2019-11-U.O), Ricerca Finalizzata (RF-2013-02358910; RF-2016-02364503), AFM-Telethon, Ateneo Sapienza University of Rome, and LBI Rehabilitation Research. Marianna Cosentino holds a fellowship from IBSA Foundation for scientific research.

Introduction

Cancer cachexia is a complex metabolic syndrome characterized by the loss of skeletal muscle mass and weakness.¹ In particular, the overwhelming majority of cancer patients (approximately 80%) presents cachexia and this wasting syndrome represents the primary cause of death in a significant fraction of patients (20–30%).^{2,3} As cancer cachexia is not usually diagnosed in early stages of the disease and radio-chemotherapy treatments can exacerbate the cachectic phenotype, loss of muscle mass can severely diminish quality of life in cancer patients.^{4,5}

To date, the underlying causes and mechanisms of cachexia are not completely understood. In this context, animal models greatly contributed to the identification of molecular networks involved in the establishment of metabolic alterations and wasting events. Nevertheless, the field has awaited the generation of appropriate *in vitro* experimental models. The aim was to limit the use of animal models, thus satisfying the principles of the 3Rs (Replacement, Reduction and Refinement) and providing a framework for performing more humane animal research, and on the other hand, to guarantee the generation of complex dynamics tissues ‘in a dish’.

Although cell lines assure consistency and simple manipulation, they cannot reproduce key *in vivo* conditions such as the complexity of host tissues and tissue–tumour interactions. Strategies involving tissue engineering have been developed to circumvent limitations of both *in vivo* and *in vitro* approaches, contributing to the study of mechanisms underlying disease onset/progression and to the identification of therapeutic targets. In particular, the design of three-dimensional (3D) engineered tissue models is currently in its development stage, showing high potential in overcoming the limitations of already available models. Indeed, the complex 3D microenvironment in which cells are organized *in vivo* allows the interaction between different cell types and between cells and the extracellular matrix; thus, 3D *in vitro* models more realistically reproduce a tissue or organ than two-dimensional (2D) cell culture systems.

Complying with these principles, in our laboratories, a scaffold-free 3D engineered skeletal muscle tissue from murine primary cultures, namely, the *ex vivo* muscle engineered tissue (X-MET), has been developed. The X-MET recapitulates, *in vitro*, morphological, molecular and functional characteristics of skeletal muscle.⁶ The X-MET is composed by a heteroge-

neous population of cells structurally organized in lengthwise disposed myotubes, connective layers and vessel-like structure, allowing nutrient diffusion.^{6,7} A key advantage of this model is the possibility to measure functional parameters such as spontaneous contraction and contractile force,^{8–10} further strengthening the rationale of using the X-MET to estimate critical outcomes of therapeutic approaches.

Currently, a pharmacologic intervention that can completely reverse the cachectic phenotype is still lacking. Hence, the importance to identify key molecular players to develop novel strategies with therapeutic potential is a critical point. Among factors, interleukin-6 (IL-6) is involved in tumour growth, malignant differentiation of cancer cells and microenvironment immunomodulation.¹¹ IL-6 has been found to be a cancer disease prognostic marker,¹² and it was also increased in patients with cancer-induced cachexia, in which it mediated the catabolic activity via signal transducer and activator of transcription 3 (STAT3) protein phosphorylation.¹³ However, IL-6 is a pleiotropic cytokine with multiple functions, ranging from homeostatic to pathogenic actions, depending on targets, levels and type of signal transduction.¹⁴

IL-6 exerts pro-inflammatory, pro-oxidant and catabolic actions, and it is sufficient to induce cachexia in mice, as well as atrophy in myotubes.¹⁵ On the other hand, IL-6 cytokine has been also recognized as a myokine, a key mediator of muscle homeostasis contributing to regenerative and hypertrophic pathways. Opposite actions of this pleiotropic mediator have been explained with the hormetic nature of its signalling and with the ability to transduce signals through different receptor complexes.¹⁴ The IL-6 classic signalling, mediated by the membrane bound receptor complex gp130/IL-6R (glycoprotein-130/IL-6 receptor), promotes anti-inflammatory and pro-regenerative actions of IL-6. In contrast, IL-6 transsignalling, mediated by IL-6 binding to the soluble IL-6R, can promote chronic inflammation and catabolic pathways.¹⁴

Based on this rationale, we built a research project (i) to generate a reliable 3D culture system to model the cancer-associated cachexia *in vitro*, (ii) to study the mechanisms underlying cancer-associated muscle wasting and (iii) to provide a useful 3D *in vitro* model as a testing tool for pharmacological treatments.

We demonstrated that X-MET recapitulates, *in vitro*, key features of the cachectic muscle phenotype when cultured in conditioned medium (CM) derived from mouse C26 colon

adenocarcinoma cells and that the cachectic activity of tumour cells is mediated by IL-6 transsignalling. Of note, pharmacologic inhibition of IL-6 transsignalling was able to counteract key phenotypic changes of cancer cachexia, including the modulation of proteolytic/autophagic pathways, the loss of muscle mass, protein content and functionality, as well as the alteration of plasma membrane.^{16–22}

Materials and methods

Experimental model

Wild-type C57Bl/6J mice and IL6RKO mice of 4 weeks of age were used to perform the experiments included in the study, in accordance with the Italian Law on the Protection of Animals. The IL6RKO murine model is a genetically modified animal constitutively knocked out of IL-6R protein expression. Specifically, to obtain the ablation of IL6R protein expression, an oligonucleotide sequence, containing a premature stop codon, has been included in the first coding exon of the *Il6r* gene by CRISPR/CAS9 technique. Furthermore, the integrated sequence introduced a restriction site recognized by EcoRI, leading to the generation of gDNA fragments utilized for mouse genotyping. Animals were hosted in a temperature-controlled (22°C) room with a 12-h light/dark cycle. The research project was conducted according to the guidelines of the Declaration of Helsinki and approved by the Institutional Review Board of the animal facilities of National Institute of Health-Italy (No. 609/2015-PR; No. 864/2020-PR).

Cell culture and media preparation

C26 colon adenocarcinoma cells, obtained from the American Type Culture Collection (ATCC; kindly provided by Prof. David Sassoon), were grown in Dulbecco's modified Eagle's medium (DMEM) with 10% foetal bovine serum (FBS), 100 U/mL of penicillin and 2 mM of L-glutamine (growth medium [GM]) and maintained at 37°C in a humidified atmosphere of 5% CO₂ in air. In order to produce C26-conditioned medium, approximately 8×10^5 C26 cells were plated in GM in a 60-mm cell culture dish (Falcon). The medium was completely replaced with 6 mL of fresh GM after the overnight attachment. When the C26 cells reached confluence, the resulting medium (C26_CM) was collected, centrifuged (1000 g for 10 min) and filtered with a 0.22- μ m polyethersulfone hydrophilic filter (Millipore). The collected medium was finally diluted in a ratio of 1:10 in the differentiation medium (DM; DMEM, 2% horse serum, 25 mM of HEPES, 4 mM of L-glutamine, 0.1% gentamicin, penicillin/streptomycin), to obtain the DM + 10% C26_CM. The medium C26_CM + glycoprotein-130 fused

chimaera (gp130Fc) was obtained by adding a concentration of 1.2 ng/mL of gp130Fc (R&D Systems) to C26_CM.

Primary culture and generation of ex vivo muscle engineered tissue

X-MET construct was obtained by mechanical and enzymatic dissociation of hind limbs of mice using the Skeletal Muscle Dissociation Kit (Miltenyi Biotec).^{6,7} Dissociated cells were filtered in a 70- μ m cell strainer and centrifuged at 250 x g for 15 min. Cells were resuspended in GM (DMEM, 20% horse serum, 3% chick embryo extract, 25 mM of HEPES, 4 mM of L-glutamine, 0.1% gentamicin, penicillin/streptomycin) and plated for 30 min twice in a row to get an enrichment of myoblasts in the culture. Cells were plated at a concentration of 40 000 cells/mL on a tissue culture dish of 35 mm diameter coated with type I collagen (Sigma-Aldrich) and incubated at 5% CO₂ at 37°C. After 5–6 days of culture, myoblasts were induced to differentiate using a DM (DMEM, 2% horse serum, 25 mM of HEPES, 4 mM of L-glutamine, 0.1% gentamicin, penicillin/streptomycin). Then, a skeletal muscle primary cell monolayer is delaminated and pinned on a silicone-coated dish (Sylgard, Dow Corning, Midland, MI, USA) using 0.20-mm-diameter stainless steel Minutien pins (Austerlitz INSECT PINS®). X-METs were cultured in DM for 3 days enabling complete remodelling in a self-organized cylindrical structure containing beating myotubes.

Then, X-METs were divided into three different groups (X-MET CTRL, X-MET treated with C26_CM and X-MET treated with C26_CM + gp130Fc compound) and treated for 5 days. We considered the samples cultured in DM with 10% of non-conditioned GM as X-MET CTRL. As described above, to simulate the cancer cachexia microenvironment, we treated X-METs with C26 cell line-conditioned medium (X-MET C26_CM). The condition X-MET C26_CM + gp130Fc was obtained by adding 1.2 ng/mL of gp130Fc to C26_CM. In detail, muscle tissue from hind limbs of one mouse will yield enough cells for fifteen 35-mm tissue culture dishes, which means an average of 15 X-MET constructs from one mouse. A total of five independent experiments were conducted, assuring a minimum of five constructs derived from different mice to perform the analysis included in the present study.

Isolation and culture of muscle stem cells and fibro-adipogenic progenitors

Satellite cell populations (MuSCs) and fibro-adipogenic progenitor cells (FAPs) were isolated by depletion of non-target cells using the Principle of the MACS® Separation (Miltenyi Biotec s.r.l.). Briefly, minced muscle was digested as described above. Then, the cell suspension was filtered using 70- μ m cell

strainers, centrifuged for 15 min at 1200 rpm and resuspended in 80 μ L of buffer (phosphate-buffered saline [PBS], pH 7.2, 0.5% FBS, 2 mM of EDTA) treated with 20 μ L of the Satellite Cell Isolation Kit per gramme of muscle for 15 min at 4°C. LS columns (Miltenyi Biotec, 130-042-401) placed in a magnetic field of a MACS Separator (Miltenyi Biotec) were used to separate the cell suspension. Unlabelled MuSCs were collected in a flow-through and purified using Anti-Integrin-7 MicroBeads (Miltenyi Biotec, 130-104-261). Then, MuSCs α -7 positive cells were plated at a density of 45 000 cells/mL in a tissue culture dish of 35 mm diameter coated with type I collagen (Sigma-Aldrich). Magnetically labelled non-satellite cells obtained from the first purification were collected in 15 mL of tubes, plated on a tissue culture dish of 100 mm diameter and incubated at 5% CO₂ at 37°C. After 48 h, cells were detached using 500 μ L of Trypsin (Sigma-Aldrich) and purified using CD140a MicroBeads Kit (Miltenyi Biotec, 130-101-502). CD140a positive cells were plated at a density of 45 000 cells/mL on a tissue culture dish of 35 mm diameter and cultured in DMEM supplemented with 10% of FBS, 1 \times penicillin/streptomycin and 2.5 ng/mL of fibroblast growth factor (FGF).

RNA extraction and real-time PCR

RNA extraction was performed using TriReagent™ (Sigma-Aldrich). The double-stranded cDNA was obtained following the retrotranscription of 1 μ g of RNA per sample, using the QuantiTect Reverse Transcription Kit (QIAGEN). Relative quantitative PCR was performed on ABI PRISM 7500 SDS (Applied Biosystems, USA), using premade 6-carboxyfluorescein (FAM)-labelled TaqMan assay for Hprt, Myh2a, Myh7, Il-6, Il6r, suppressor of cytokine signalling 3 (Socs3), ATROGIN1, muscle ring finger-1 (MuRF1), cathepsin L (Ctsl), light chain 3 (LC3), tumour necrosis factor α (Tnfa), interleukin-1 β (Il1b), cyclin K (Ccnk), cyclin-dependent kinase inhibitor 2a (Cdkn2a), Bcl2-associated X protein (Bax) and B cell leukaemia/lymphoma 2 (Bcl2) (Applied Biosystems). The Hprt mRNA expression was used to normalize the relative quantitative real-time (RT)-PCR sample value. To assess the expression of microRNAs (miR-1, miR-206, miR-133a, miR-21, miR-24, miR-31 and miR-34c), the extracted RNA was retrotranscribed using microRNA Reverse Transcription Kit (Applied Biosystems). Relative quantitative PCR was performed on ABI PRISM 7500 SDS (Applied Biosystems) as described above, and the relative quantitative RT-PCR sample value was normalized for the expression of U6 snRNA.

Immunofluorescence analysis

Immunofluorescence analysis was performed on the entire amount of X-MET. It was fixed with 4% paraformaldehyde

(PFA) for 15 min, washed in PBS with 1% bovine serum albumin (BSA) and 0.2% Triton X-100, preincubated for 1 h in 10% donkey serum at room temperature (RT) and incubated overnight at 4°C with MF20 (Sigma-Aldrich) and cleaved caspase 3 (Cell Signaling) antibodies. X-METs were then washed in PBS with 0.2% Triton X-100 and incubated with a secondary antibody (Alexa Fluor, Life Technologies) for 45 min at RT. Nuclei were stained using HOECHST. Images were taken with a Nikon DS-Fi1 camera (Nikon Corporation, Tokyo, Japan) coupled with a Zeiss Axiovert optical microscope (Zeiss, Oberkochen, Germany). For each experimental condition, three independent experiments were performed.

Protein extraction and western blot

Total protein extract was obtained by homogenizing each sample in lysis buffer (Tris-HCL, pH 7.5/20 mM, EDTA/2 mM, EGTA/2 mM, sucrose/250 mM, DTT/5 mM, Triton-X/0.1%, PMSF/1 mM, NaF/10 mM, SOV4/0.2 mM, Cocktail Protease Inhibitors/1 \times) (Sigma-Aldrich). The same quantities of protein (70 μ g) from each lysate, quantified through the Bradford assay, were then electrophoresed in sodium dodecyl sulfate (SDS) polyacrylamide gel (4–15% Criterion™ TGX Stain-Free™ Protein Gel, Bio-Rad). Proteins were transferred into a nitrocellulose membrane (Trans-Blot Turbo transfer pack, Bio-Rad) using the Trans-Blot® Turbo™ Transfer System (programme: 1.3 A, 25 V, 7 min). The membrane was then blocked with 5% BSA in TBS-1% Tween for 1 h at RT, followed by an incubation with diluted antibody for STAT3 (Cell Signaling), phosphorylated STAT3 (pSTAT3) (Cell Signaling), MF20 (Sigma-Aldrich), β -actin (Sigma A3854) and sarcomeric actin (Antibodies A36150) in blocking solution overnight at 4°C. After washing in TBS-1% Tween, the membrane was incubated with a specific peroxidase-conjugated secondary antibody and then visualized by the enhanced chemiluminescence system (ChemiDoc Imaging System, Bio-Rad). The acquired signal was evaluated by scanning densitometry using a bio-image analysis system (Image Lab™ Software). The results were expressed as relative integrated intensity compared with controls (GAPDH), and the ratio of relative intensities of pSTAT3 to total STAT3 was measured to assess STAT3 pathway activation.

Enzyme-linked immunosorbent assay

Aliquots of culture supernatant from C26 adenocarcinoma cell line were collected after 3 days and compared with fresh DM. IL-6 and IL6R levels were then assayed using the DuoSet ELISA Development System (DY406-05 and DY1830) following the instructions provided by the manufacturer. The optical density of each sample was determined using a microplate reader set to 450 nm (Digital and Analog System).

Functional characterization of the ex vivo muscle engineered tissue models

We performed different functional tests to analyse the bio-mechanical properties of the X-MET models with the aim to validate this construct as a suitable model to study cancer-associated muscle wasting, as well as to test the efficacy of the gp130Fc protein in mediating cancer-related loss of skeletal muscle functionality. At first, we evaluated the frequency of the tissue's spontaneous contraction during the 5 days of treatment by using an optical tracking algorithm developed in LabView 2019.^{8,23,24} The images of the X-MET models were acquired at 300 fps for 10 s and then correlated by the algorithm in a region of interest (ROI) of 600 × 90 pixels, divided in 18 nodes and placed in the centre of the construct. The spontaneous contraction frequency was then computed through the fast Fourier transform (FFT). The use of the FFT allowed obtaining the amplitude of the signal components at each analysed frequency, thus finding the main signal component that characterizes the tissue's contraction. Then, on the last day of conditioning, we measured the spontaneous contraction force of the X-MET models and the force generated by the constructs during a stimulation protocol constituted by one twitch test with a 1-ms single pulse stimulation and two tetanic stimulations delivered at 40 and 80 Hz. For all the tests, the force was measured through the use of a microforce transducer (Kronex AE801)^{8–10} and the specific spontaneous forces were obtained by dividing the acquired force for the cross-sectional area (CSA) of the tissues, calculated with a programme developed in Matlab.⁸ For the entire duration of the functional tests, the X-MET models were maintained at a temperature of 37°C, by using a temperature control plate (Okolab s.r.l., H401).

Evans Blue dye

X-METs, pinned in a silicon-coated dish, were treated with 1% Evans Blue dye (EBD) (Sigma E2129) (w/v) in PBS (pH 7.5) filtered using Millex®-GP 0.22 µm of filter (Millipore, Bedford, MA, USA). Evans Blue is a non-permeating dye, which is used for checking cell viability and plasma membrane damage. Images were obtained using Axio Imager A2 microscope (Carl Zeiss Microimaging, Inc.) and processed by ZEN2 software (Blue Edition). The evaluation of EBD-derived fluorescence was performed on at least five fields chosen arbitrarily from each sample and was analysed by ImageJ software.

Statistical analyses

Statistical significance was determined by using one-way analysis of variance (ANOVA), two-way ANOVA and unpaired *t*-test with GraphPad Prism 8.0 software (Graph Pad

Software Inc., La Jolla, CA, USA). Differences between groups were determined by Tukey's multiple comparisons test and Bonferroni's test. Asterisks denote statistically significant differences. Statistical significance was set to a *P* value < 0.05.

Results

The ex vivo muscle engineered tissue model recapitulates, in vitro, key features of the cachectic muscle phenotype

Based on the complex and not completely understood aetiopathogenesis of cachexia, we validated the 3D X-MET in vitro construct as a suitable model to study cancer-associated muscle wasting. To this aim, we used CM derived from mouse C26 colon adenocarcinoma cells, a cellular model that induces cancer cachexia in mice, to study the morpho-functional properties and molecular mechanisms underlying muscle wasting in X-MET construct.^{6,10,25}

As the X-MET has been characterized as a skeletal muscle-like structure,⁶ we at first evaluated the weight of the whole construct as an index of potential loss of muscle mass. We observed, after 5 days in a C26-conditioned medium, a significant reduction of the whole X-MET mass compared with the control medium (*Figure 1A*).

As a significant impairment of myosin expression has been observed both in rodent cancer models and in cachectic cancer patients,^{26–28} we analysed fast 2a myosin heavy chain (Myh2a) and slow myosin heavy chain isoform (Myh7) gene expression in our 3D model. We observed that the X-MET cultured in presence of C26-derived CM showed a significant down-regulation of both Myh2a and Myh7 gene expression compared with control (*Figure 1B*). The negative regulation of Myh genes induced by C26_CM in the X-MET model was further associated with a significant decrease in myosin protein content, compared with control construct (*Figure 1C*). We further reported a significant reduction of β-actin (*Figure 1C*) and skeletal muscle actin (*Figure 1D*) proteins in the X-MET C26_CM compared with control, indicating that factors derived from C26 tumour cells directly affect the X-MET construct, impairing muscle protein content. To evaluate whether the loss of structural and contractile proteins observed in the X-MET C26_CM would impair the force generating ability of the construct, we performed a functional test to analyse the X-MET spontaneous contraction frequency. As revealed by the optical tracking analysis, control X-METs displayed a functional frequency of ~4 Hz while the X-METs cultured with C26-conditioned medium showed an almost complete impairment of the contraction frequency (*Figure 1E*).

These data indicated that the factors released by C26 cancer cells directly affect skeletal muscle robustness and functionality and highlighted the X-MET model as a valid muscle-like

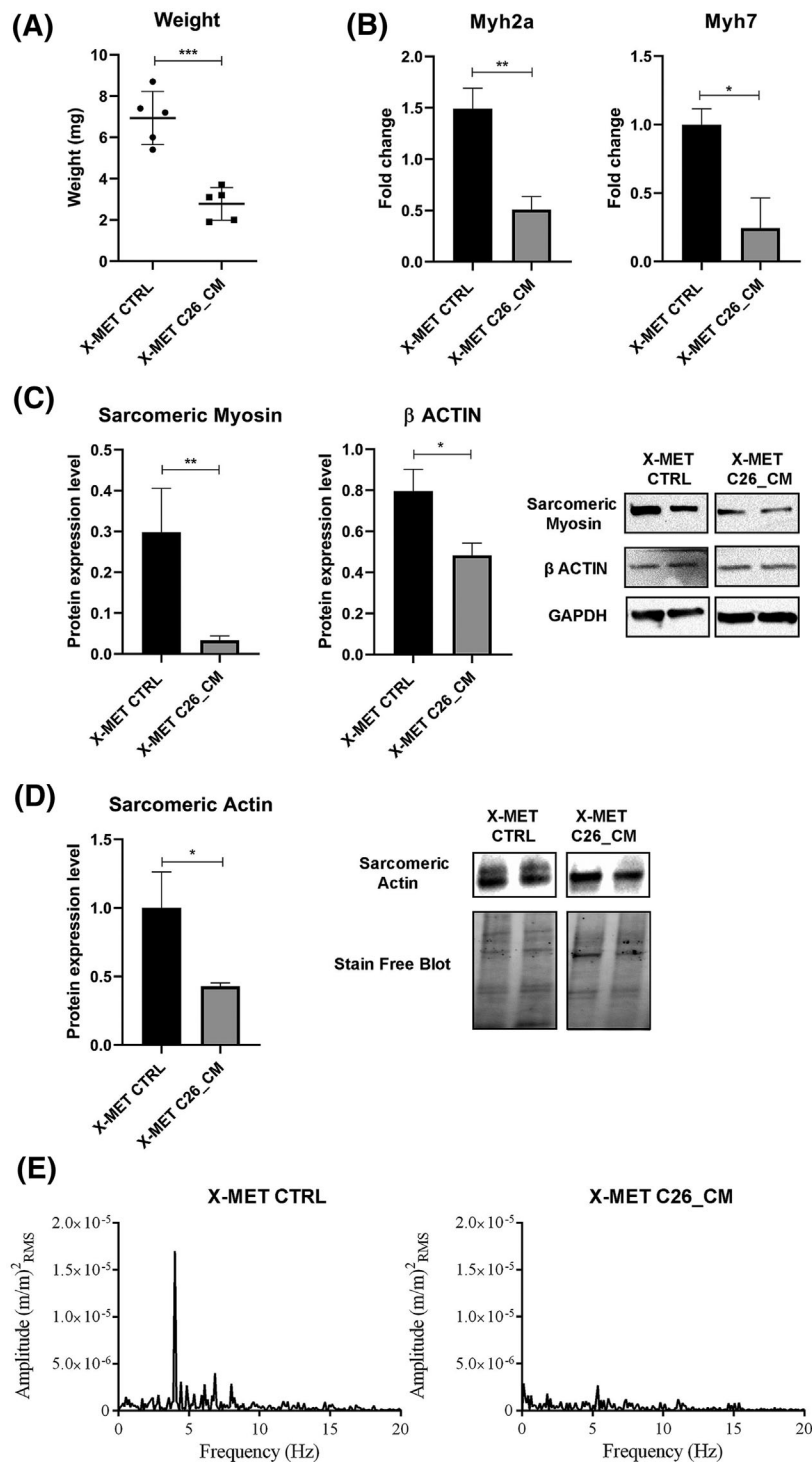


Figure 1 The ex vivo muscle engineered tissue (X-MET) recapitulates in vitro typical features of cancer cachexia, exhibiting a significant decline of structural components and altered contractile properties. (A) Histogram shows the weight measurements (mg) of control X-METs (CTRL) and X-METs treated with C26-conditioned medium (C26_CM). The values represent mean \pm SEM of five independent experiments, unpaired *t*-test ($*P < 0.05$, $**P < 0.005$, $***P < 0.001$). (B) Quantitative expression of myosin heavy chain genes (Myh2a and Myh7) measured by quantitative real-time PCR (qRT-PCR). The values represent mean \pm SEM of five independent experiments, unpaired *t*-test ($P < 0.05$) ($n \geq 4$ per group). HPRT was used for the normalization. (C) Representative western blot bands (right panel) and densitometric analysis (left panel) of sarcomeric myosin and β -actin expression ($n \geq 5$ per group). All data are expressed as a mean \pm SEM. (D) Densitometric analysis (left panel) and representative western blot bands (right panel) of sarcomeric actin expression ($n \geq 3$ per group). All data are expressed as a mean \pm SEM. (E) Representative frequency spectrum obtained during spontaneous contraction for X-MET CTRL (left) and X-MET C26_CM (right).

model able to reflect, *in vitro*, key features of the cachectic phenotype.

C26-derived conditioned medium induced interleukin-6 signalling in the ex vivo muscle engineered tissue model through the release of both interleukin-6 and soluble IL6R

Increased levels of circulating pro-inflammatory cytokines have been suggested as potential causative factors for cachexia.²⁹ Among them, IL-6 is thought to correlate to the cachectic condition being a recognized mediator of pro-inflammatory, pro-oxidant, catabolic and degenerative pathways.

To evaluate the potential involvement of IL-6 as a determinant in the establishment of a cachectic phenotype in the X-MET construct, we investigate whether IL-6 signalling is induced in our model.

We at first evaluated, by enzyme-linked immunosorbent assay (ELISA), the content of IL-6 cytokine and IL6R in tissue culture media. We observed that the medium conditioned by C26 tumour cells contains elevated levels of both IL-6 and soluble IL6R when compared with fresh control medium (Figure 2A).

As C26 cells secreted elevated levels of both IL-6 and IL6R, we investigated whether the IL-6 signal transduction was activated in the X-MET construct upon conditioning with C26-derived medium. Interestingly, the expression of both IL-6 and IL6r genes was also significantly induced in the C26_CM-treated X-MET compared with control X-MET (Figure 2B). Thus, we analysed the activation of STAT3 by evaluating the phosphorylated active form of the protein (pY705-STAT3). We revealed a significant increase of pSTAT3/STAT3 ratio in the C26_CM-treated X-MET, compared with control cell culture (Figure 2C).

As IL-6 is a pleiotropic cytokine with multiple functions, ranging from homeostatic to pathogenic effects, we wondered whether the detrimental action of IL-6 signal stimulation on the X-MET construct would be mainly associated with the induction of the transsignalling rather than the classic signalling. To validate this hypothesis, we generated the X-MET from an IL6RKO mouse model, characterized by the constitutive lack of IL6R protein expression. By using C26_CM as a unique source of soluble IL6R protein within the X-MET IL6RKO model, we evaluated the specific response of muscle tissue to cancer-induced IL-6 transsignalling. We observed a significant decline of tissue mass in the IL6RKO construct after the administration of C26-conditioned medium (X-MET IL6RKO C26_CM), compared with untreated control X-MET IL6RKO culture system (Figure 3A). In accordance with the loss of tissue mass, we observed a decline of myosin genes expression (Myh2a and Myh7) in the IL6RKO X-MET (Figure 3B) and a significant up-regulation of ATROGIN1 and MuRF1 gene expression (Figure 3C), master regulators of the ubiquitin–proteasome

pathway, upon C26-conditioned medium administration, confirming the prominent role of IL-6 transsignalling in inducing a cachectic-like phenotype. Furthermore, we observed that the administration of C26-derived medium to the X-MET IL6RKO induced pro-apoptotic changes in the X-MET IL6RKO culture system, with a significant down-modulation of Bcl2 gene and the enhancement of Bax gene expression compared with controls (Figure 3D).

Interleukin-6 transsignalling blockade is sufficient to counteract the pro-cachectic action of C26-derived conditioned medium on the ex vivo muscle engineered tissue construct

As IL-6 is a pleiotropic cytokine with multiple functions, ranging from homeostatic to pathogenic actions, we wondered whether the detrimental action of IL-6 signal stimulation on the X-MET construct would be mainly associated with the induction of the transsignalling rather than the classic signalling. To validate this hypothesis, we used the X-MET conditioned with C26-derived medium as an *in vitro* model of tumour-induced muscle wasting. In this model, we tested the efficacy of the gp130Fc protein in interfering with the induction of pathologic changes in a muscle-like structure. A dose of 1.2 ng/mL of gp130Fc has been added to the C26-conditioned medium to culture the mature X-MET. Five days after treatment, the X-MET constructs were collected and analysed for molecular and morpho-functional parameters.

To verify whether gp130Fc treatment was able to modulate IL-6 signal transduction induced by C26-conditioned medium in the X-MET, we analyse the activation of STAT3 protein and the expression of Socs3 gene. We reported that the X-MET C26_CM showed a reduction in pSTAT3/STAT3 ratio upon gp130Fc treatment compared with the untreated construct (Figure 4A). In accordance, Socs3 gene expression, which is known to be induced by IL-6 through the STAT3 pathway, was reduced in the X-MET C26_CM treated with gp130Fc compared with the untreated X-MET (Figure 4B). Interestingly, the activation of STAT3 and the expression of Socs3 gene returned to basal levels in the X-MET conditioned with C26 medium and treated with gp130Fc. In order to further validate the efficacy of gp130Fc neutralizing activity, we measured the levels of free IL6R protein in X-METs media collected at the experimental endpoint (5 days of treatment). The ELISA revealed that the medium derived from X-METs conditioned with C26_CM contained elevated levels of IL6R protein compared with untreated X-MET (Figure 4C). Conversely, gp130Fc administration to the X-MET C26_CM significantly reduced the levels of free IL6R in supernatant (Figure 4C). These data confirmed the effective modulation of IL-6 signal transduction induced by gp130Fc protein.

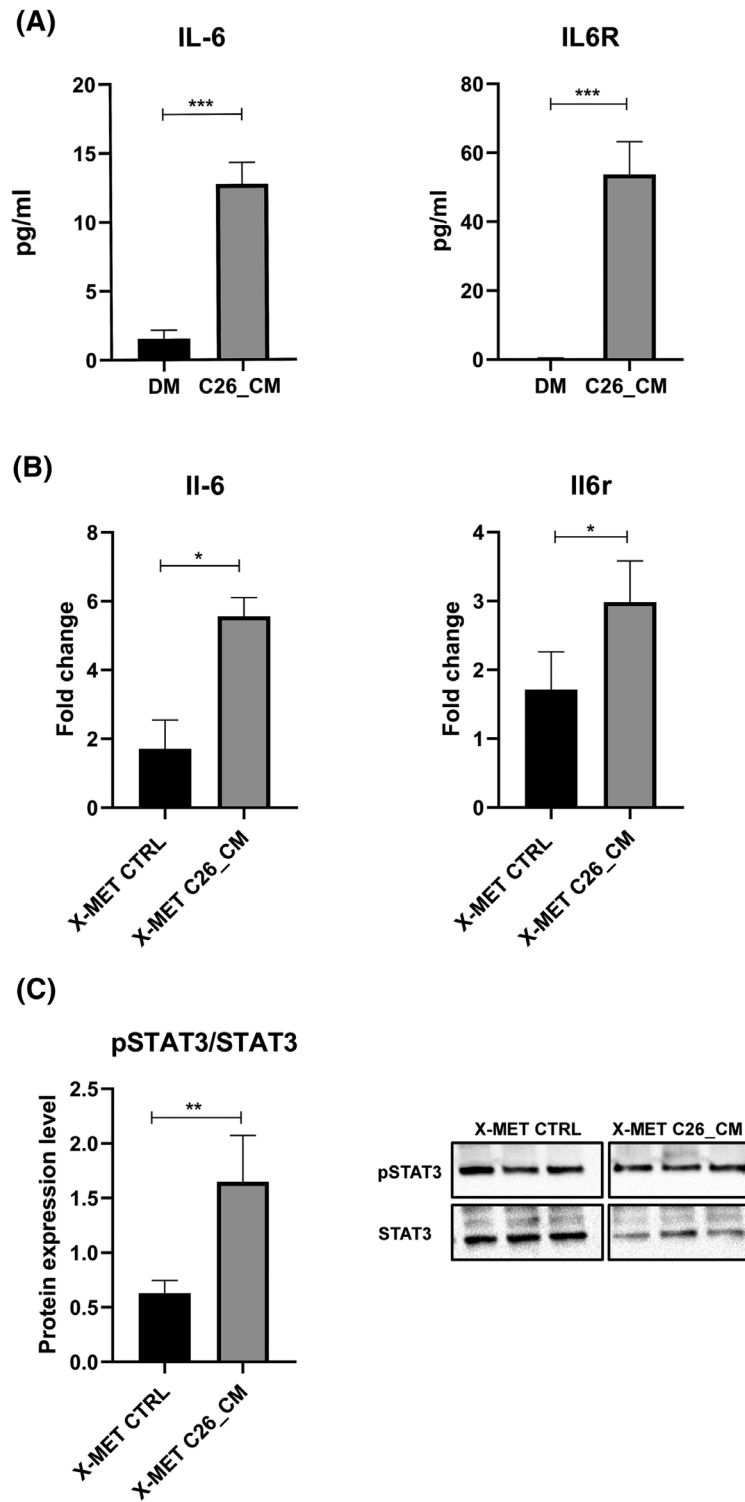


Figure 2 C26-conditioned medium induced the activation of interleukin-6 (IL-6) signal transduction in the ex vivo muscle engineered tissue (X-MET) model. (A) Histogram shows the concentration (pg/mL) of IL-6 and IL6R measured by enzyme-linked immunosorbent assay comparing the differentiation medium (DM) and C26-conditioned medium (C26_CM). The values represent mean \pm SEM. (B) Histogram shows the expression of II-6 and II6r for X-MET control (CTRL) and X-MET treated with C26_CM measured by quantitative real-time PCR (qRT-PCR). The values represent mean \pm SEM of five independent experiments, unpaired *t*-test ($P < 0.05$) ($n \geq 4$ per group). HPRT was used for the normalization. (C) Densitometric analysis (left panel) and representative western blot bands (right panel) of the phosphorylated signal transducer and activator of transcription 3 (pSTAT3) and signal transducer and activator of transcription 3 (STAT3) expression ($n \geq 6$ per group). Graph to the left shows quantitative analyses of replicative blots of the ratio of relative intensities of pSTAT3 to total STAT3 in X-MET CTRL and X-MET C26_CM. All data are expressed as a mean \pm SEM.

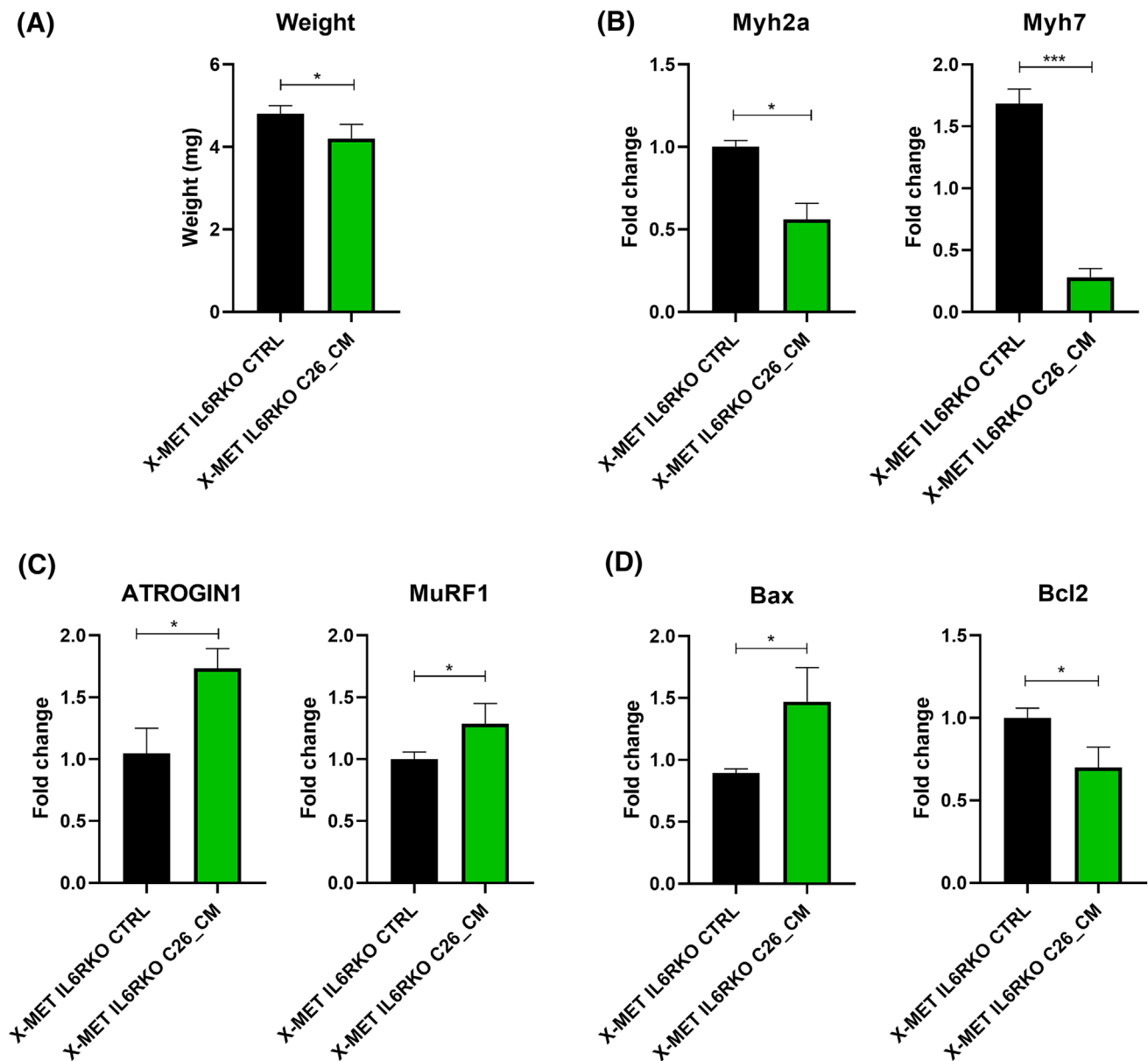


Figure 3 C26-conditioned medium induces cachectic changes in the ex vivo muscle engineered tissue (X-MET) IL6RKO construct. (A) Histogram shows the weight measurements (mg) of control IL6RKO X-METs and IL6RKO X-METs treated with C26-conditioned medium. The values represent mean \pm SEM of three independent experiments, unpaired *t*-test ($*P \leq 0.05$). (B–D) Quantitative expression of myosin heavy chain genes (Myh2a and Myh7) (B), ATROGIN1 and muscle ring finger-1 (MuRF1) (C), and Bcl2-associated X protein (Bax) and B cell leukaemia/lymphoma 2 (Bcl2) (D) genes measured by quantitative real-time PCR (qRT-PCR). The values represent mean \pm SEM; *P* value by unpaired *t*-test ($P < 0.05$). HPRT was used for the normalization.

We proceeded with morpho-functional and molecular analysis to investigate whether the interference with IL-6 transsignalling could protect the X-MET against the establishment of a cachectic phenotype induced by C26-conditioned medium. At first, we evaluated the impact of gp130Fc treatment on the CSA of the X-MET conditioned with C26 medium. We observed that C26-derived medium induced a significant reduction of the whole X-MET CSA compared with control (Figure 4D). In contrast, no differences were observed

in the X-MET C26_CM treated with gp130Fc compared with control (Figure 4D).

We thus evaluated whether blocking IL-6 transsignalling would influence proteolytic pathways. We observed a significant induction of ATROGIN1 and MuRF1, master regulator of the ubiquitin–proteasome pathway, in the X-MET conditioned with C26-derived medium compared with the control medium (Figure 4E). The supplementation of gp130Fc protein to X-MET C26_CM significantly reduced the expression of

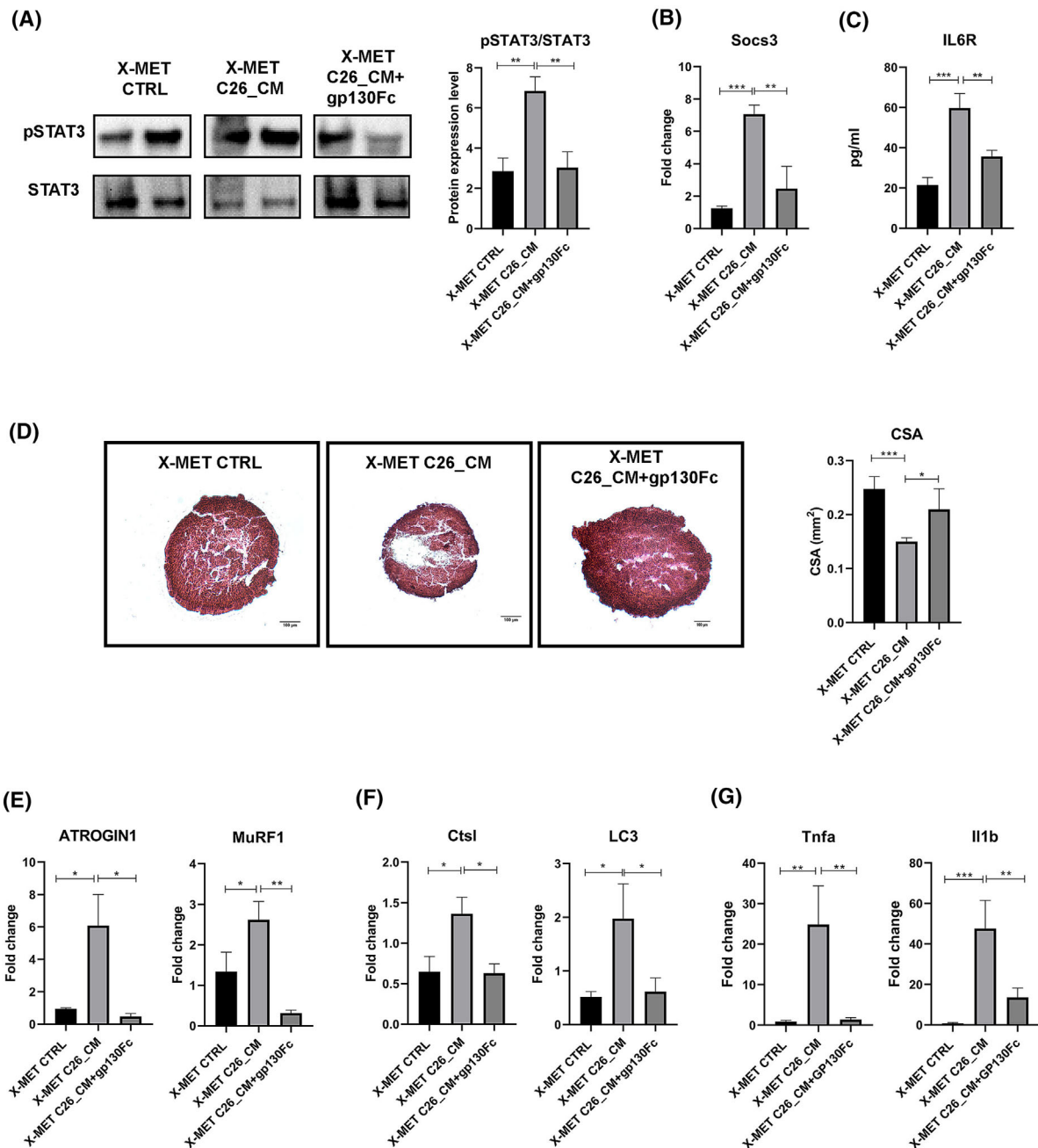


Figure 4 Interleukin-6 (IL-6) transsignalling blockade counteracts the establishment of cachectic alterations in the ex vivo muscle engineered tissue (X-MET) model. (A) Representative western blot bands (left panel) and densitometric analysis (right panel) of the phosphorylated signal transducer and activator of transcription 3 (pSTAT3) and signal transducer and activator of transcription 3 (STAT3) expression ($n \geq 6$ per group). Graph to the right shows quantitative analyses of replicative blots of the ratio of relative intensities of pSTAT3 to total STAT3 in X-MET CTRL, X-MET C26_CM and X-MET C26_CM + glycoprotein-130 fused chimaera (gp130Fc), respectively. All data are expressed as a mean \pm SEM. (B) Quantitative real-time PCR (qRT-PCR) analysis for the expression of suppressor of cytokine signalling 3 (Socs3) gene ($n \geq 6$ per group). HPRT was used for the normalization. All data are expressed as a mean \pm SEM. *P* values were calculated using one-way analysis of variance test, and Bonferroni's test was used for multiple comparisons (* $P < 0.05$, ** $P < 0.01$, *** $P < 0.001$, **** $P < 0.0001$). (C) Histogram shows the concentration (pg/mL) of IL6R measured by enzyme-linked immunosorbent assay comparing the X-MET control medium (X-MET CTRL), the X-MET C26-conditioned medium (X-MET C26_CM) and the X-MET C26 medium plus gp130Fc (X-MET C26_CM + gp130Fc) at the endpoint of the treatment. The values represent mean \pm SEM. *P* values were calculated using one-way analysis of variance test (** $P < 0.01$, *** $P < 0.001$). (D) Haematoxylin and eosin staining on cross sections of treated and non-treated X-METs (left panel) and measure of corresponding cross-sectional area (right panel). All data are expressed as a mean \pm SEM ($n \geq 4$ per group). (E–G) Histograms show the expression of ATROGIN1 and muscle ring finger-1 (MuRF1) (E), cathepsin L (Ctsl) and light chain 3 (LC3) (F), and tumour necrosis factor α (Tnfa) and interleukin-1 β (Il1b) (G) measured by qRT-PCR. HPRT was used for the normalization. All data are expressed as a mean \pm SEM ($n \geq 4$). *P* values were calculated using one-way analysis of variance test (* $P < 0.05$, ** $P < 0.01$, *** $P < 0.001$, **** $P < 0.0001$).

both ATROGIN1 and MuRF1 gene expression, compared with the untreated X-MET C26_CM (Figure 4E). A similar expression pattern has been observed also for markers of the autophagy–lysosome system. In particular, we observed that the C26-derived medium induced a significant up-regulation of Ctsl, and the microtubule-associated protein 1 LC3 gene expression compared with the control medium (Figure 4F). In contrast, in the X-MET C26_CM treated with gp130Fc, the expression of both Ctsl and LC3 genes (Figure 4F) remains at basal levels, highlighting the relevance of IL-6 transsignalling in inducing cancer-associated muscle proteolysis and wasting. Interestingly, we also found that the Tnfa and the Il1b, cytokines primarily involved in the enhancement of catabolism in cachectic patients,³⁰ were both down-modulated in the X-MET C26_CM treated with gp130Fc compared with the X-MET C26_CM (Figure 4G).

Activation of interleukin-6 transsignalling impinges satellite cells activity

It has been demonstrated that cachectic mice exhibit a deficit in muscle stem cell proliferation and differentiation.³¹ To verify which cell populations, myofiber itself or other cell populations, are affected by IL-6 transsignalling activation in the muscle, we isolated myogenic and non-myogenic progenitors from wild-type murine muscles. MuSCs and FAPs were separately cultured and then treated with CM derived from mouse C26 colon adenocarcinoma cells. Morpho-functional and molecular analysis demonstrated an impairment of MuSCs differentiation in presence of C26 medium compared with control MuSCs and C26_CM MuSCs treated with gp130Fc (Figure 5A). At first, we observed that the length of myotubes was reduced in presence of C26_CM compared with control medium while gp130Fc administration efficiently counters the impact of tumour-derived factors (Figure 5B). Sarcomeric myosin expression was down-regulated in myotubes treated with C26_CM compared with control medium, while physiologic levels of expression were maintained in culture treated with C26_CM plus gp130Fc (Figure 5C,G). We further observed that the supplementation of gp130Fc compound to C26_CM myotubes was sufficient to normalize the expression of both ATROGIN1 and MuRF1 genes that were significantly enhanced in C26_CM-treated myotubes compared with controls (Figure 5D). We confirmed the pro-apoptotic impact of C26 medium on myotubes and the protective role exerted by IL-6 transsignalling blockade. Indeed, the C26-conditioned medium significantly alters the expression of apoptotic genes (Bax and Bcl2) on differentiated MuSCs, and it induces the expression of caspase 3 (Figure 5E,G). In contrast, the expression of pro- and anti-apoptotic genes and caspase 3 expression was rescued by neutralizing IL-6/sIL-6R complex (Figure 5E,G), suggesting that the tumour-dependent induction of IL-6 transsignalling plays a direct role in disturbing

molecular networks of myogenic cell homeostasis further eliciting a negative effect on mature myofibers. As FAPs are known to promote MuSC proliferation and to influence the commitment of myoblasts to terminal differentiation,²² we investigated whether tumour-derived factors can affect FAPs survival. Isolated FAPs were treated with C26-derived medium with or without the supplementation of gp130Fc compound. We observed that FAPs were not significantly influenced by C26-conditioned medium or gp130Fc administration as shown by the expression levels of key mediators of the apoptotic programme (Figure 5F).

Interleukin-6 transsignalling blockade improves the functional properties of cachectic ex vivo muscle engineered tissue

To further strengthen these results, we use the X-MET model to perform functional tests analysing the spontaneous contraction frequency. Figure 6A shows the amplitudes of FFT analysis corresponding to the main frequency components of the spontaneous force signals. Two-way ANOVA showed a significant reduction, among all the acquisition days, in C26_CM X-MET models, compared with the untreated ones. Of note, gp130Fc treatment promotes a significant functional rescue of the X-METs treated with C26_CM. Interestingly, a post hoc test showed no significant difference of the FFT amplitudes between the X-METs treated with gp130Fc and the untreated ones, expressed 96 h after the beginning of the treatment, confirming that the pharmacological treatment allowed tissues to develop a more synchronous spontaneous contraction. The measurements of the specific spontaneous forces (Figure 6B) were performed on four X-METs for each analysed condition, in the last day of the treatment, showing values of 1.61 ± 1.12 , 2.09 ± 0.56 and 2.73 ± 0.93 mN/mm² for C26_CM X-MET, X-MET treated with gp130Fc and untreated X-MET, respectively. These results demonstrated better functionality in the constructs treated with gp130Fc with respect to the tissue cultured with C26-conditioned medium, with an increase of the generated force of ~29%. Figure 6C shows the specific twitch and tetanic force developed by the constructs in the last day of the treatment. One-way ANOVA showed an increase of the developed forces in the tissues treated with gp130Fc statistically higher than those developed by the tissues treated with C26_CM, for both twitch and tetanic forces. Interestingly, for the tetanic stimulation, we measured a maximum tetanic force of 4.23 ± 2.04 , 23.77 ± 16.23 and 28.92 ± 4.31 mN/mm² for X-MET C26_CM, X-MET C26_CM treated with gp130Fc and untreated X-MET, respectively.

The loss of structural and sarcomeric proteins can lead not only to an impaired muscle functionality but also to the alteration of sarcolemma stability. To investigate this aspect, based also on the evidence that cancer cachexia can cause skeletal

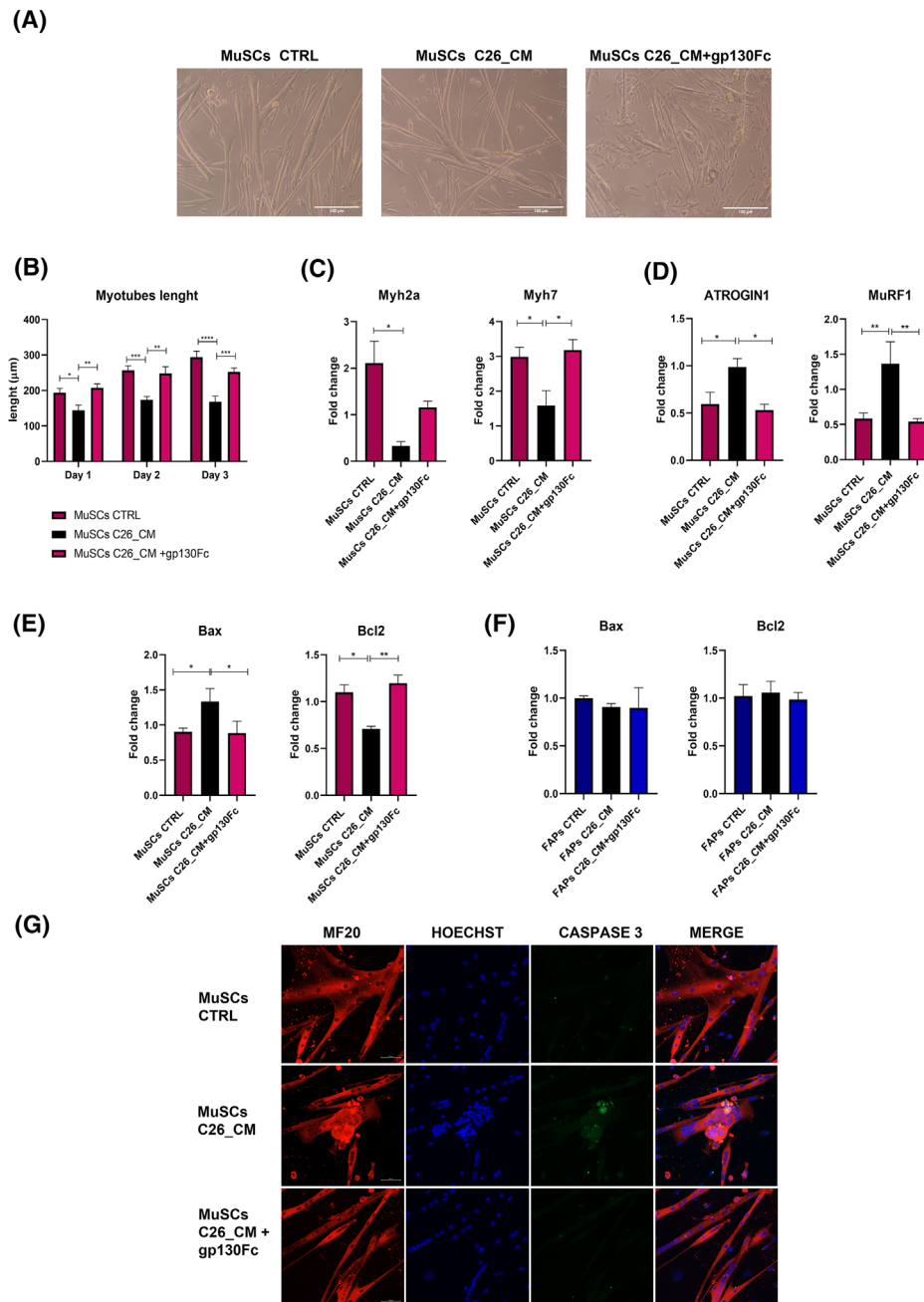


Figure 5 The tumour-dependent stimulation of interleukin-6 (IL-6) transsignalling alters satellite cell activity. (A) Representative brightfield images of differentiated satellite cell populations (MuSCs) cultured in control medium, with C26-conditioned medium (C26_CM) and in presence of C26_CM plus glycoprotein-130 fused chimaera (gp130Fc). Magnification $\times 10$. (B) Quantification of myotubes length at the indicated time points and experimental conditions. The analysis has been performed by using ImageJ software. All data are expressed as a mean \pm SEM ($n = 5$), and P values were calculated by two-way analysis of variance ($*P < 0.05$, $**P < 0.01$, $***P < 0.001$, $****P < 0.0001$). (C–E) Histograms show the expression of myosin genes (C; Myh2a and Myh7), atrophic markers (D; ATROGIN1 and muscle ring finger-1 [MuRF1]) and apoptotic genes (E; Bcl2-associated X protein [Bax] and B cell leukaemia/lymphoma 2 [Bcl2]) in differentiated MuSCs upon administration of C26-conditioned medium alone or in combination with gp130Fc protein compared with control medium. Gene expression has been measured by quantitative real-time PCR (qRT-PCR). HPRT was used for the normalization. All data are expressed as a mean \pm SEM. P values were calculated using one-way analysis of variance test ($*P < 0.05$, $**P < 0.01$, $***P < 0.001$, $****P < 0.0001$). (F) Histograms show the expression of apoptotic genes (Bax and Bcl2) in fibro-adipogenic progenitor cells (FAPs) upon administration of C26-conditioned medium alone or in combination with gp130Fc protein compared with control medium. Gene expression has been measured by qRT-PCR. HPRT was used for the normalization. All data are expressed as a mean \pm SEM. (G) Representative images of MF20 (anti-myosin antibody) immunostaining (Alexa 568, red signal), nuclei staining (HOECHST, blue signal) and cleaved caspase 3 (Alexa 488, green signal) for control differentiated MuSCs (CTRL), MuSCs treated with C26-conditioned medium (C26_CM) and MuSCs cultured with C26-CM and treated with gp130Fc (C26_CM + gp130Fc) ($\times 20$ magnification).

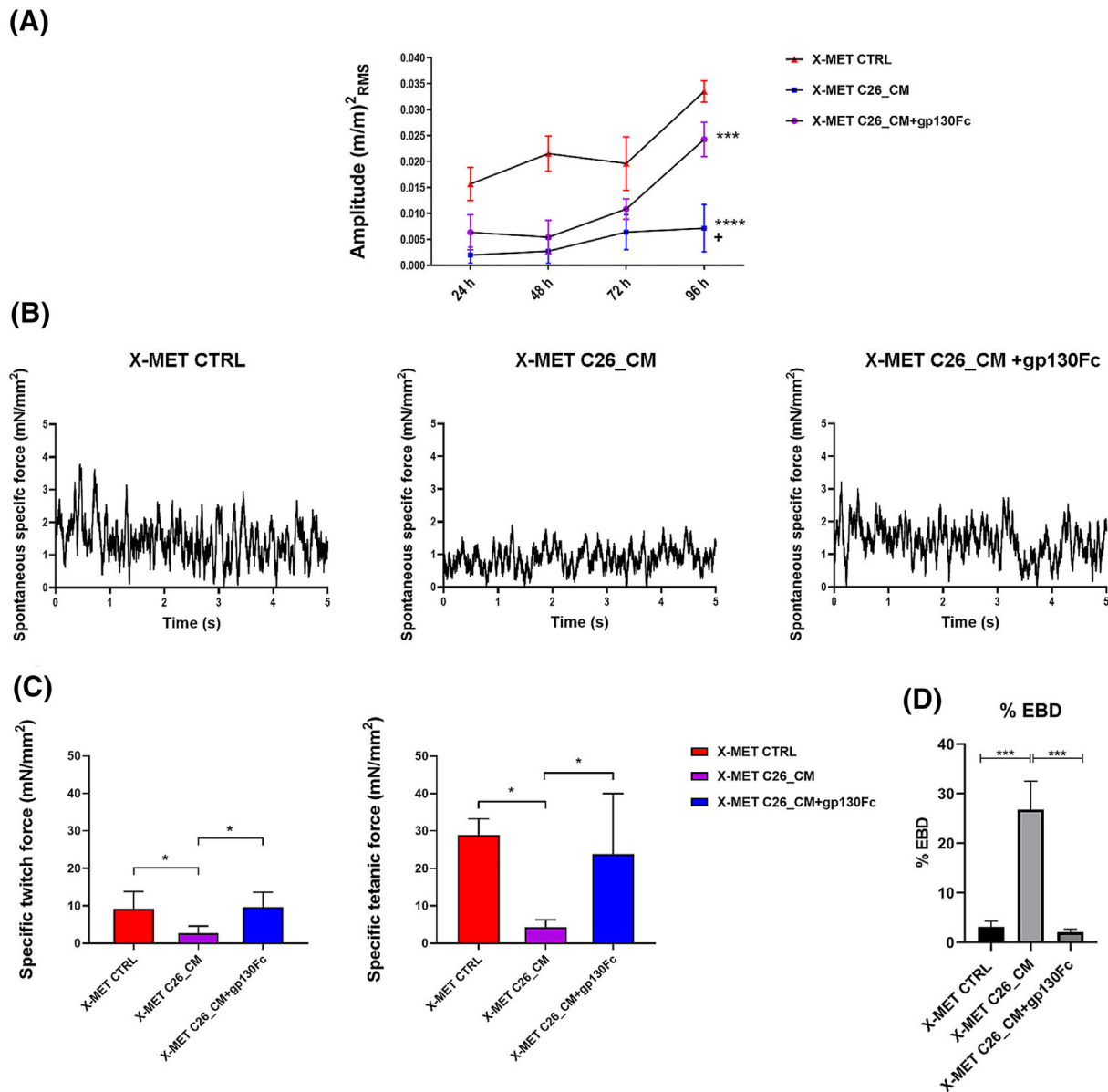


Figure 6 Pharmacological inhibition of interleukin-6 (IL-6) transsignalling preserves muscle function against tumour-induced cachexia. (A) Main frequency components amplitude of the ex vivo muscle engineered tissues (X-METs) spontaneous contraction for control X-MET (CTRL), X-MET treated with C26-conditioned medium (C26_CM) and X-MET cultured with C26-CM and treated with glycoprotein-130 fused chimaera (gp130Fc) protein (C26_CM + gp130Fc) during the entire duration of the treatments. Data are expressed as mean \pm SEM ($n \geq 4$). P values were calculated using two-way analysis of variance test (*** $P < 0.001$, **** $P < 0.0001$ vs. X-MET CTRL, * $P < 0.05$ vs. X-MET C26_CM + gp130Fc). (B) Representative X-MET-specific spontaneous contraction force acquired at the fifth day of treatment with average peak-to-peak values of 2.26, 1.45 and 1.80 mN/mm² for X-MET CTRL, X-MET C26_CM and X-MET C26_CM + gp130Fc, respectively. (C) Specific twitch force (Ftw/CSA) and maximum specific tetanic force acquired at the fifth day of treatment for X-MET CTRL, X-MET C26_CM and X-MET C26_CM + gp130Fc. All data are expressed as mean \pm SD ($n \geq 3$). P values were calculated using two-way analysis of variance test (* $P < 0.05$). (D) Densitometric analysis from confocal microscopy images of Evans Blue dye (EBD) fluorescence for control X-MET (X-MET CTRL), X-MET treated with C26-conditioned medium (X-MET C26_CM) and X-MET cultured with C26-CM and treated with gp130Fc (X-MET C26_CM + gp130Fc) ($\times 20$ magnification; 50 μ m of scale bar); quantification of EBD positive area for each condition. All data are expressed as a mean \pm SEM. P values were calculated using one-way analysis of variance test (*** $P < 0.001$).

muscle damage, we evaluated, by EBD uptake, the alteration of muscle fibre integrity after contraction (Figure 6D). X-MET constructs, treated with C26-conditioned medium alone or in combination with gp130Fc and control ones, have been electrically stimulated to induce the generation of the tetanic

force and stained with EBD. Confocal microscopy analysis of EBD fluorescence in the whole X-MET revealed a significant increase of EBD uptake by the X-MET treated with C26-conditioned medium compared with control (Figure 6D). The administration of gp130Fc to the X-MET C26_CM signifi-

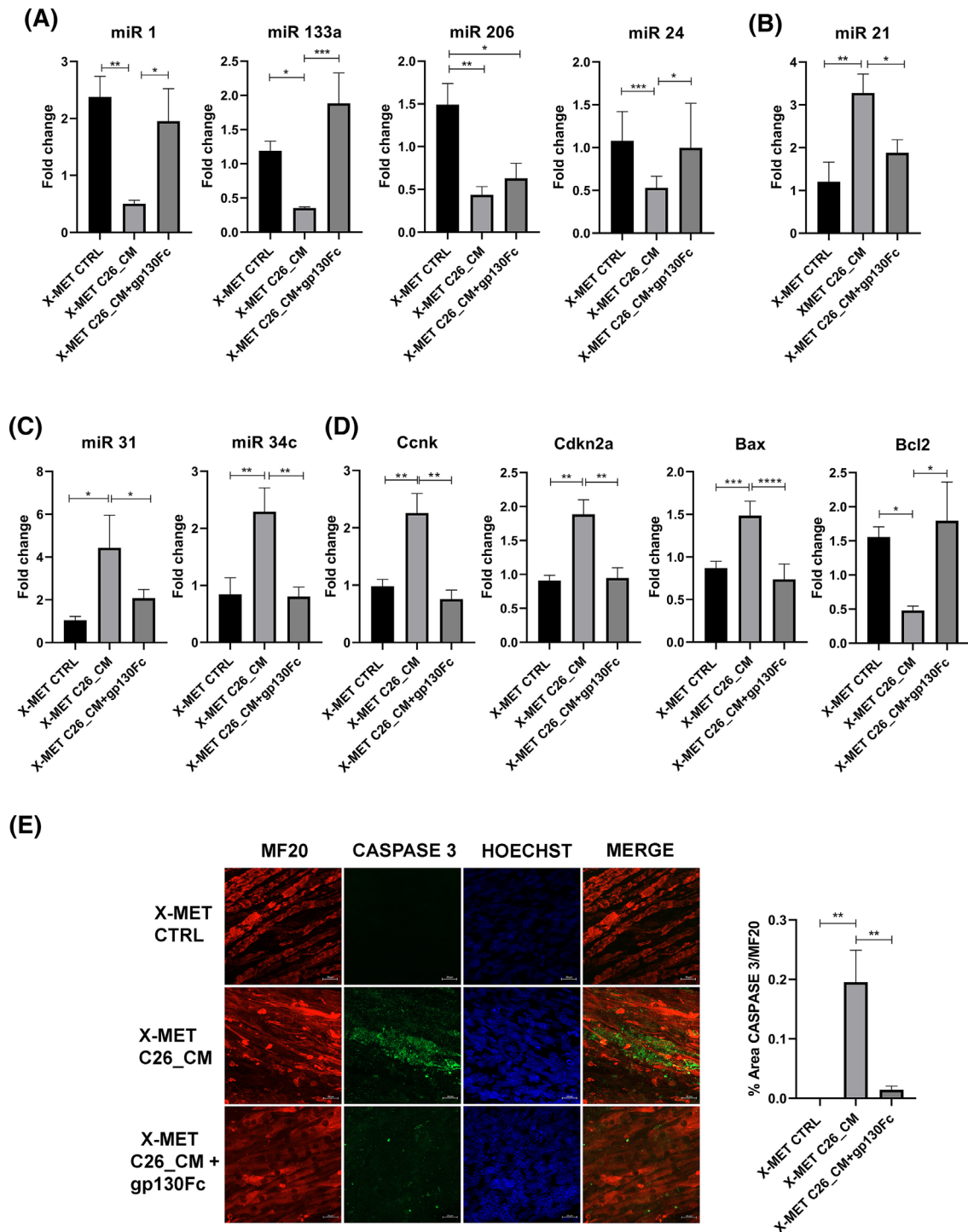


Figure 7 Interleukin-6 (IL-6) transsignaling neutralization modulates gene regulatory networks involved in myogenesis and apoptosis. Histograms show the expression of miR-1, miR-133a, miR-206 and miR-24 (A), miR-21 (B), miR-31 and miR-34c (C), cyclin K (Ccnk), cyclin-dependent kinase inhibitor 2a (Cdkn2a), Bcl2-associated X protein (Bax) and B cell leukaemia/lymphoma 2 (Bcl2) genes (D) measured by quantitative real-time PCR (qRT-PCR). U6 and HPRT were used for miRNA and gene expression normalization, respectively. All data are expressed as a mean \pm SEM ($n \geq 4$). P values were calculated using one-way analysis of variance test (* $P < 0.05$, ** $P < 0.01$, *** $P < 0.001$, **** $P < 0.0001$). (E) Immunofluorescence analyses of MF20 (Alexa 568, red signal), cleaved caspase 3 (Alexa 488, green signal) and nuclei staining (HOECHST, blue signal) for control ex vivo muscle engineered tissue (X-MET) (CTRL), X-MET treated with C26-conditioned medium (C26_CM) and X-MET cultured with C26-CM and treated with glycoprotein-130 fused chimaera (gp130Fc) (C26_CM + gp130Fc). Representative images obtained by confocal microscopy ($\times 40$ magnification; 20 μ m of scale bar) (left panel); quantification of green area (cleaved caspase 3) related to red area (MF20) for each condition (right histogram). All data are expressed as a mean \pm SEM ($n \geq 5$). P values were calculated using one-way analysis of variance test (* $P < 0.05$, ** $P < 0.01$, *** $P < 0.001$, **** $P < 0.0001$).

cantly reduced the percentage of EBD fluorescence within myofibers, raising control levels (Figure 6D).

Glycoprotein-130 fused chimaera protein rescues the deregulated expression pattern of microRNAs associated with myogenesis and apoptosis induced by C26-derived medium in the ex vivo muscle engineered tissue construct

Muscle-specific miRNAs (myomiRs), regulating myogenesis and contributing to muscle homeostasis, have been involved in metabolic alterations associated with cancer cachexia. Thus, we evaluated the expression pattern of muscle-specific microRNAs in the 3D culture system, under the different experimental conditions. We observed a significant reduction of relevant myomiRs, namely, miR-1, miR-133a and miR-206, in the X-MET cultured with the C26-derived medium compared with control medium (Figure 7A). On the other hand, we observed that gp130Fc supplement to C26 medium induced an up-regulation of myomiRs in the X-MET construct when compared with C26-conditioned medium (Figure 5A). Of note, in the X-MET C26_CM treated with gp130Fc, the expression of muscle-specific microRNAs, except for miR-206, was raised to control levels (Figure 7A).

Regarding non-muscle-specific microRNAs involved in the homeostatic maintenance of skeletal muscle tissue, we analysed the expression of positive and negative regulators of myogenesis such as miR-24 and miR-21, as well as the expression of apoptotic miRNAs, miR-31 and miR-34c. The X-MET showed a significant down-modulation of miR-24 upon conditioning with C26-derived medium compared with control medium. On the other hand, miR-24 expression in the X-MET C26_CM supplemented with gp130Fc protein was comparable with basal levels (Figure 7A).

We observed a significant up-regulation of miR-21 in the X-MET cultured with C26-conditioned medium compared with control medium, while the treatment with gp130Fc brought the expression of miR-21 back to control levels in the X-MET C26_CM (Figure 7B). These data suggest that tumour-derived factors, with reference to IL-6 signalling components, can affect the homeostatic maintenance of muscle tissue by disturbing the expression pattern of myogenic microRNAs.

We further reported a similar expression pattern for other non-muscle-specific microRNAs, namely, miR-31 and miR-34c, associated with the promotion of apoptotic processes and which are known to be induced in damaged myofibers.^{32–34} In particular, miR-31 and miR-34c were significantly induced in the X-MET cultured with C26-conditioned medium compared with control, while the expression of both miRNAs was comparable with basal levels in presence of gp130Fc protein (Figure 7C).

To better investigate whether the inhibition of IL-6 transsignalling in the X-MET C26_CM could counter the induction of apoptotic pathways, we analysed the mRNA levels of Bcl2, BCL2-associated X protein (BAX), Ccnk and Cdkn2a. We observed that the C26-conditioned medium significantly induces the expression of the pro-apoptotic genes Bax, Ccnk and Cdkn2a in the X-MET, while the anti-apoptotic gene Bcl2 was dramatically reduced in the X-MET C26_CM compared with control constructs. The X-MET C26_CM treated with gp130Fc showed expression levels of Bax, Bcl2, Ccnk and Cdkn2a comparable with the control construct, indicating a protective role of IL-6 transsignalling inhibition against the induction of pro-apoptotic pathways (Figure 7D). In accordance, analysis of transversal sections of the whole X-MET by confocal microscopy revealed a widespread expression of caspase 3, a key apoptotic protease, in X-MET C26_CM but not in the construct supplemented with gp130Fc or cultured with control medium (Figure 7E).

Discussion

Cancer cachexia has been defined as ‘a complex metabolic syndrome associated with underlying illness and characterised by loss of muscle with or without loss of fat mass’.³⁵ The occurrence of this syndrome is known to dramatically affect cancer patient quality of life and has been associated with a reduced response to chemotherapy and overall survival. To date, no therapies are available to reverse the progressive and massive loss of skeletal muscle, which is considered the main feature of cancer cachexia. A wealth of studies has been performed in experimental models to identify and target potential triggers of the cancer cachexia, greatly improving the knowledge about mechanisms underlying this syndrome. Unfortunately, a comprehensive understanding of pathogenic mechanisms is still lacking and the consensus on the use of experimental models.³⁶ Both in vivo and in vitro approaches presented intrinsic and extrinsic limitations as they are simplified models of a complex syndrome, associated with different types of tumours and occurring in a multifaceted spectrum of patients with different degrees of illness severity and comorbidities. However, experimental models are necessary to clarify mechanisms driving pathogenic events and, with reference to in vitro models, are useful for direct drug screening, reducing the use of animal models and saving costs and time. Based on this rationale, we proposed a 3D engineered skeletal muscle, the X-MET, as a novel model that recapitulates muscle diseases and tested the efficacy of therapeutic compounds.⁶ This model, previously characterized and standardized,^{6,7} appears as a reliable tool presenting important advantages other than the main features of classical cell-based models: (i) It presents morpho-functional properties closely resembling

in vivo skeletal muscle tissue; (ii) the heterogeneous cell population composing the construct allows the formation of an organized architecture of muscle, endothelial and connective tissue, increasing the level of complexity of classical 2D in vitro models; and (iii) it is possible to accurately measure spontaneous contraction, force and mechanical power,^{9,10} assessing the efficacy of therapeutic treatments in terms of functional parameters.

Taking advantage of X-MET characteristics, we investigated the impact of cancer-associated induction of IL-6 signalling on muscle tissue with a dual aim: (i) to assess the direct action of IL-6 and its signalling molecules in inducing cachexia-like effects and (ii) to assure that the X-MET would respond to cancer-derived factors displaying the main features of cachexia.

C26 adenocarcinoma tumour cells have been used as a source of soluble factors contributing to the establishment of cancer cachexia. In particular, C26 cancer cells are known to release elevated levels of IL-6 cytokine, which has been functionally associated with cachexia in murine models.^{37–39}

We observed that the X-MET exposed to medium conditioned by mouse C26 colon adenocarcinoma cells showed a significant decline in morpho-functional properties along with the alteration of molecular mechanisms of protein degradation. In particular, the significant reduction of mass in the X-MET cultured with C26-conditioned medium was accompanied by the dramatic decline of myosin and actin expression compared with control construct. The sensible decline of structural components in the X-MET upon conditioning with tumour-derived factors reflected the enhancement of protein degradation pathways that are known to contribute to muscle wasting in cachexia. Evidence deriving from in vivo and in vitro studies has reported the alteration of sarcomeric mRNA and protein levels under cachectic conditions,^{26–28} and it is well known that myosin and actin are the major sarcomere contractile proteins, responsible for force generation during contraction.⁴⁰ Of note, reduced content of sarcomeric proteins was associated with the impairment of contractile properties of the X-MET. This aspect is of particular relevance because monitoring muscle mass and functionality is considered as an essential point to strengthen preclinical studies in cancer cachexia.³⁶ Thus, these data validated the X-MET as a reliable experimental model recapitulating in vitro the main features of cancer-induced muscle wasting.

Once validating the establishment of pathogenic changes in the X-MET construct cultured with cancer medium, we tested our model as a tool for drug screening.

In order to investigate mechanisms triggering cancer-associated muscle wasting and to select a targetable pathway, we focused on IL-6 signal transduction. A wealth of studies reported the pivotal role of cancer-derived IL-6, and its signal transduction, in contributing to cachexia syndrome. Indeed, IL-6 has been recognized as sufficient to induce cachexia in mice, and in a recent article, Rupert and colleagues¹⁵ defined

an IL-6 transsignalling loop between tumour, muscle and fat exacerbating muscle wasting in pancreatic ductal adenocarcinoma (PDAC) cachexia.^{14,37,38} In accordance, we reported high levels of both IL-6 and IL-6R in medium derived from C26 cells activating IL-6 signal transduction in the X-MET construct and possibly inducing a feed-forward loop of IL-6 and IL6R expression. Indeed, the X-MET cultured in presence of high-level IL-6 and IL6R not only showed a significant induction of STAT3 activity but also increased levels of both IL-6 and IL6r gene expression in the muscle construct. Within this context, it is worth reporting that the activation of STAT3 has been defined as necessary and sufficient for muscle wasting in cancer cachexia.³⁷ Our data indicated that C26 tumour cells are able to secrete high levels of both IL-6 and IL6R that can in turn activate IL-6 signal transduction in muscle cells. Furthermore, the induction of IL-6 and IL-6R expression in C26_CM stimulated construct suggested the induction of a feed-forward loop of IL-6 signalling.

Based on these observations, we asked whether the cachectic-like phenotype observed in the C26_CM-treated X-MET would be mainly ascribed to the impact of IL-6 transsignalling instead of classic signalling. To answer this question, we generated the X-MET from an IL6RKO mouse model, characterized by the constitutive lack of IL6R protein expression. Hence, the X-MET IL6RKO does not express the IL6R protein and thus presents a complete ablation of both IL-6 classic and transsignalling. By adding C26_CM to the IL6RKO X-MET, we were able to evaluate the specific response of muscle tissue to cancer-induced IL-6 transsignalling, as in this model, the only source of sIL6R mediating IL-6 transsignalling comes from the C26-conditioned medium. We observed a significant decline of tissue mass in the X-MET IL6RKO after the administration of C26-conditioned medium, compared with untreated control X-MET IL6RKO. In accordance with the loss of tissue mass, we observed, similarly to what we reported for the wild-type X-MET, a significant up-regulation of atrophic markers and a decline of myosin genes expression in the X-MET IL6RKO upon C26-conditioned medium administration, confirming the prominent role of IL-6 transsignalling in inducing a cachectic-like phenotype. Furthermore, we observed that the administration of C26-derived medium to the X-MET IL6RKO induced pro-apoptotic changes in the X-MET IL6RKO culture system. Altogether, these data corroborate the hypothesis that IL-6 transsignalling represents a dominant mediator of muscle decline induced by cancer-derived medium.

To investigate the direct impact of IL-6 transsignalling in muscle tissue, spared from the influence of other tissues that would be targets of cancer factors, we used the X-MET model and a molecular approach to neutralize soluble IL6R action. We used the gp130Fc protein to selectively thwart IL-6/sIL6R complex activity, without affecting the activity of IL-6 cytokine through the classic signalling. Our results showed that the interference with IL-6 transsignalling in the C26-derived

medium was sufficient to antagonize the pro-degenerative action of cancer-conditioned medium on the whole X-MET model and on isolated muscle stem cells. In particular, gp130Fc supplementation to cancer-conditioned X-MET prevented the loss of muscle tissue, normalizing proteolytic pathways and thus preserving the robustness of the muscle construct. The beneficial effect of IL-6 transsignalling blockade was further highlighted by the improved tissue functionality and the reduced sensibility to mechanical stress in the X-MET C26_CM treated with gp130Fc. Altogether, these data confirm the ability of gp130Fc compound to modulate proteasome-mediated proteolysis and auto-phagocytosis process, closely linked to muscle wasting under cachectic conditions. This protective action of IL-6 transsignalling blockade against the pathologic loss of structural and contractile proteins preserves muscle mass, sarcolemma integrity and myofiber functionality.

Along with the modulation of classical pathways, well described in cancer cachexia, we further reported a differential modulation of non-coding RNAs in the X-MET treated with gp130Fc. Interestingly, mounting evidence supports the role of microRNAs in triggering or amplifying cancer-associated muscle wasting.⁴¹ It has been reported that tumour-derived factors, including pro-inflammatory cytokines, can affect peripheral and central metabolic pathways contributing to cancer cachexia. In this context, it has been highlighted that microRNAs can influence metabolic regulation directly or by affecting cytokines. Among them, myomiRs, regulating myogenesis and contributing to muscle homeostasis, have been involved in metabolic alterations associated with cancer cachexia.

About that, we showed that C26-conditioned medium induced a significant impairment of myogenic microRNAs (miR-1, miR-133a and miR-206) in the X-MET. In contrast, the expression profile of miR-1 and miR-133a was restored by treating the X-MET C26_CM with gp130Fc. As myomiRs contribute to the robustness of the myogenic programme,⁴² the loss of these regulatory mediators might contribute to alter the stability of the X-MET in presence of cancer-derived factors. The ability of gp130Fc treatment to restore myogenic miRNA expression in the X-MET could suggest the existence of an inhibitory network, mediated by IL-6 transsignalling, affecting the generation and maintenance of a robust muscle tissue. Other microRNAs, although not muscle specific, have been recognized as key mediators involved in the homeostatic maintenance of skeletal muscle tissue.^{32,43,44} Among them, miR-24 has been associated with the maintenance of the differentiated phenotype of myofibers, being highly expressed in terminally differentiated muscle tissue.⁴³ MiR-21 is known to be induced by pro-inflammatory and pro-oxidant stimuli, and it has been reported as a negative regulator of myogenesis contributing to muscle wasting by reducing myoblast viability and myogenic potential.⁴⁵ In addition, miR-21 is a well-characterized oncogenic microRNA that

is overexpressed in several malignancies, and it has been proposed as a biomarker of prognosis and as a therapeutic target. Other non-muscle-specific microRNAs, miR-31 and miR-34c, have been associated with the promotion of apoptotic processes and are known to be induced in damaged myofibers.^{33,34,37} If myogenic miRNA expression was impaired, a significant enhancement of microRNA involved in pro-apoptotic and damage-associated pathways has been observed in the X-MET C26_CM. In particular, microRNAs such as miR-21, miR-31 and miR-34c have been found overexpressed in the X-MET conditioned with C26 medium. Otherwise, miR-24 was significantly reduced by C26 conditioning, suggesting an impaired maintenance of the differentiated phenotype in myofibers subject to cachectic stimuli.

In line with the described role of these miRNAs in inducing apoptotic pathways, the cancer-conditioned X-MET showed high levels of apoptotic markers, suggesting that cancer-derived factors can dramatically affect muscle tissue leading to muscle cell death. Interestingly, also, in this case, the selective neutralization of IL-6 transsignalling normalized the expression of miRNAs and of the overall the analysed mediators, resulting in the strong reduction of cleaved caspase 3.

Altogether, these data are in accordance with the classical view of cancer-induced muscle wasting, in which tumour-associated deregulation of pro-inflammatory mediators sensibly affects muscle cells leading to catabolic and apoptotic events. Furthermore, we highlighted how IL-6 transsignalling stimulated by cancer cells could directly affect muscle tissue. The detrimental action of IL-6 transsignalling was not associated only with the recognized catabolic role of the cytokine but also to a profound alteration of muscle stability leading to the loss of tissue robustness and to the induction of apoptotic pathways.

Overall, our data suggest that the X-MET model could be considered a reliable tool for preclinical studies and that the selective inhibition of IL-6 transsignalling is a promising strategy to protect muscle tissue against the extensive wasting characterizing cancer cachexia. It has been reported that IL-6 activity can be completely blocked using the neutralizing monoclonal antibody. Nevertheless, this potential therapeutic approach blocks both classic and transsignalling. In contrast, we provide evidence that interfering with IL-6 transsignalling can have more translational clinical impact. Indeed, we were able to selectively block the IL-6 transsignalling, by the application of the gp130Fc compound, a recombinant protein able to selectively block IL-6 transsignalling by neutralizing IL-6 cytokine in complex with the soluble IL6R, without interfering with the classic signalling. As a strategy, this offers a number of clear advantages because administration of gp130Fc will not result in a complete suppression of all IL-6 responses, which may have more widespread clinical ramifications. Thus, interfering with IL-6 transsignalling will be a promising strategy for the treatment of cachectic patients.

Acknowledgements

We thank Marisa Di Giuseppe and Andrea Pirrottina for the technical support and Prof. Zaccaria Del Prete for providing materials and advice. The authors of this manuscript certify that they comply with the ethical guidelines for authorship and publishing in the *Journal of Cachexia, Sarcopenia and Muscle*.⁴⁶

References

- Roberts BM, Frye GS, Ahn B, Ferreira LF, Judge AR. Cancer cachexia decreases specific force and accelerates fatigue in limb muscle. *Biochem Biophys Res Commun* 2013;**435**:488–492.
- Fearon KCH, Glass DJ, Guttridge DC. Cancer cachexia: mediators, signaling, and metabolic pathways. *Cell Metab* 2012;**16**:153–166.
- Narsale AA, Carson JA. Role of IL-6 in cachexia—therapeutic implications. *Curr Opin Support Palliat Care* 2014;**8**:321–327.
- Shadrin IY, Khodabukus A, Bursac N. Striated muscle function, regeneration, and repair. *Cell Mol Life Sci* 2016;**73**:4175–4202.
- Allen DG, Kentish JC. The cellular basis of the length-tension relation in cardiac muscle. *J Mol Cell Cardiol* 1985;**17**:821–840.
- Carosio S, Barberi L, Rizzuto E, Nicoletti C, Del Prete Z, Musarò A. Generation of ex vivo-vascularized muscle engineered tissue (X-MET). *Sci Rep* 2013;**3**:1420.
- Cosentino M, Nicoletti C, Valenti V, Schirone L, Di Nonno F, Apa L, et al. Remodeled ex vivo muscle engineered tissue improves heart function after chronic myocardial ischemia. *Sci Rep* 2023;**13**:10370.
- Apa L, Cosentino M, Forconi F, Musarò A, Rizzuto E, Del Prete Z. The development of an innovative embedded sensor for the optical measurement of ex-vivo engineered muscle tissue contractility. *Sensors* 2022;**22**:6878.
- Pisu S, Apa L, Cosentino M, Musarò A, Rizzuto E, Del Prete Z. Measuring the X-MET's maximum power: a preliminary study. *IEEE Int Symp Med Meas Appl Proc* 2018, MeMeA 2018, 1–5.
- Pisu S, Cosentino M, Apa L, Musarò A, Rizzuto E, Del Prete Z. Measuring the maximum power of an ex vivo engineered muscle tissue with isovelocity shortening technique. *IEEE Trans Instrument Measure* 2019;**68**:1404–1411.
- Uygun A, Lee RT. Mechanisms of cardiac regeneration. *Dev Cell* 2016;**36**:362–374.
- Porrello ER, Mahmoud AI, Simpson E, Hill JA, Richardson JA, Olson EN, et al. Transient regenerative potential of the neonatal mouse heart. *Science* 2011;**331**:1078–1080.
- Beltrami AP, Barlucchi L, Torella D, Baker M, Limana F, Chimenti S, et al. Adult car-
- diac stem cells are multipotent and support myocardial regeneration. *Cell* 2003;**114**:763–776.
- Forcina L, Franceschi C, Musarò A. The hormetic and hermetic role of IL-6. *Ageing Res Rev* 2022;**80**:101697.
- Rupert JE, Narasimhan A, Jengelley DHA, Jiang Y, Liu J, Au E, et al. Tumor-derived IL-6 and trans-signaling among tumor, fat, and muscle mediate pancreatic cancer cachexia. *J Exp Med* 2021;**218**:e20190450.
- Saini A, Faulkner S, Al-Shanti N, Stewart C. Powerful signals for weak muscles. *Ageing Res Rev* 2009;**8**:251–267.
- Attaix D, Ventadour S, Codran A, Béchet D, Taillandier D, Combaret L. The ubiquitin-proteasome system and skeletal muscle wasting. *Essays Biochem* 2005;**41**:173–186.
- Li Y, Schwartz RJ, Waddell ID, Holloway BR, Reid MB. Skeletal muscle myocytes undergo protein loss and reactive oxygen-mediated NF- κ B activation in response to tumor necrosis factor α . *FASEB J* 1998;**12**:871–880.
- Burckart K, Beca S, Urban RJ, Sheffield-Moore M. Pathogenesis of muscle wasting in cancer cachexia: targeted anabolic and anti-catabolic therapies. *Curr Opin Clin Metab Care* 2010;**13**:410–416.
- Forcina L, Miano C, Scicchitano BM, Musarò A. Signals from the niche: insights into the role of IGF-1 and IL-6 in modulating skeletal muscle fibrosis. *Cell* 2019;**8**:232.
- Sutantdyo N. The role of microRNA in cancer cachexia and muscle wasting: a review article. *Caspian J Intern Med* 2021;**12**:124–128.
- Forcina L, Miano C, Pelosi L, Musarò A. An overview about the biology of skeletal muscle satellite cells. *Curr Genomics* 2019;**20**:24–37.
- Apa L, Martelli F, Rizzuto E, Del Prete Z. Design of a new device to measure skeletal muscle engineered tissues' contractile force by using an optical tracking technique. *Med Meas Appl* 2019, MeMeA 2019 - Symp Proc, 1–5.
- Forconi F, Apa L, Cosentino M, Musarò A, Rizzuto E, Del Prete Z. Effects of ROI positioning on the measurement of engineered muscle tissue contractility with an optical tracking method. *IEEE Int Symp Med Meas Appl* 2022, MeMeA 2022 - Conf Proc, 1–5.

Conflict of interest statement

The authors declare that they have no competing interests.

Data Availability Statement

The datasets used and/or analysed during the current study are available from the corresponding author on reasonable request.

- Bonetto A, Rupert JE, Barreto R, Zimmers TA. The colon-26 carcinoma tumor-bearing mouse as a model for the study of cancer cachexia. *J Vis Exp* 2016;54893. <https://doi.org/10.3791/54893>
- Banduseela V, Ochala J, Lamberg K, Kalimo H, Larsson L. Muscle paralysis and myosin loss in a patient with cancer cachexia. *Acta Myol* 2007;**26**:136–144.
- Norman H, Zackrisson H, Hedström Y, Andersson P, Nordquist J, Eriksson LI, et al. Myofibrillar protein and gene expression in acute quadriplegic myopathy. *J Neurol Sci* 2009;**285**:28–38.
- Diffey GM, Kalfas K, Al-Majid S, McCarthy DO. Altered expression of skeletal muscle myosin isoforms in cancer cachexia. *Am J Physiol Cell Physiol* 2002;**283**:1376–1382.
- Webster JM, Kempen LJAP, Hardy RS, Langen RCJ. Inflammation and skeletal muscle wasting during cachexia. *Front Physiol* 2020;**11**:597675.
- Cole CL, Kleckner IR, Jatoi A, Schwarz EM, Dunne RF. The role of systemic inflammation in cancer-associated muscle wasting and rationale for exercise as a therapeutic intervention. *JCSM Clin Reports* 2018;**3**:1–19.
- Inaba S, Hinohara A, Id MT, Tsujikawa K, Fukadaid S-I. Muscle regeneration is disrupted by cancer cachexia without loss of muscle stem cell potential. *PLoS ONE* 2018;**13**:e0205467.
- Greco S, De Simone M, Colussi C, Zaccagnini G, Fasanaro P, Pescatori M, et al. Common micro-RNA signature in skeletal muscle damage and regeneration induced by Duchenne muscular dystrophy and acute ischemia. *FASEB J* 2009;**23**:3335–3346.
- Guo JT, Wang L, Yu HB. MiR-31 aggravates inflammation and apoptosis in COPD rats via activating the NF- κ B signaling pathway. *Eur Rev Med Pharmacol Sci* 2020;**24**:9633–9644.
- Pelosi L, Coggi A, Forcina L, Musarò A. MicroRNAs modulated by local mIGF-1 expression in mdx dystrophic mice. *Front Aging Neurosci* 2015;**7**:69.
- Evans WJ, Morley JE, Argilés J, Bales C, Baracos V, Guttridge D, et al. Cachexia: a new definition. *Clin Nutr* 2008;**27**:793–799.
- Penna F, Busquets S, Argilés JM. Experimental cancer cachexia: evolving strategies

- for getting closer to the human scenario. *Semin Cell Dev Biol* 2016;**54**:20–27.
37. Bonetto A, Aydogdu T, Jin X, Zhang Z, Zhan R, Puzis L, et al. JAK/STAT3 pathway inhibition blocks skeletal muscle wasting downstream of IL-6 and in experimental cancer cachexia. *Am J Physiol Endocrinol Metab* 2012;**303**:E410–E421.
38. Chen JL, Walton KL, Qian H, Colgan TD, Hagg A, Watt MJ, et al. Differential effects of IL6 and activin A in the development of cancer-associated cachexia. *Cancer Res* 2016;**76**:5372–5382.
39. Baltgalvis KA, Berger FG, Peña MMO, Davis JM, White JP, Carson JA. Muscle wasting and interleukin-6-induced atrogen-1 expression in the cachectic *Apc^{Min/+}* mouse. *Pflugers Arch Eur J Physiol* 2009;**457**:989–1001.
40. Yin Z, Ren J, Guo W. Sarcomeric protein isoform transitions in cardiac muscle: a journey to heart failure. *Biochim Biophys Acta* 2015;**1852**:47–52.
41. Marceca GP, Nigita G, Calore F, Croce CM. MicroRNAs in skeletal muscle and hints on their potential role in muscle wasting during cancer cachexia. *Front Oncol* 2020;**10**:2604.
42. Gagan J, Dey BK, Dutta A. MicroRNAs regulate and provide robustness to the myogenic transcriptional network. *Curr Opin Pharmacol* 2012;**12**:383–388.
43. Sun Q, Zhang Y, Yang G, Chen X, Zhang Y, Cao G, et al. Transforming growth factor- β -regulated miR-24 promotes skeletal muscle differentiation. *Nucleic Acids Res* 2008;**36**:2690–2699.
44. Eisenberg I, Alexander MS, Kunkel LM. miRNAs in normal and diseased skeletal muscle. *J Cell Mol Med* 2009;**13**:2–11.
45. Borja-Gonzalez M, Casas-Martinez JC, McDonagh B, Goljanek-Whysall K. Inflammation-miR-21 negatively regulates myogenesis during ageing. *Antioxidants* 2020;**9**:345.
46. von Haehling S, Morley JE, Coats AJS, Anker SD. Ethical guidelines for publishing in the Journal of Cachexia, Sarcopenia and Muscle: update 2021. *J Cachexia Sarcopenia Muscle* 2021;**12**:2259–2261.